VOL. 10, NO. 21, NOVEMBER 2015 ISSN 1819-6608
ARPN Journal of Engineering and Applied Sciences


www.arpnjournals.com

MODELING AND ANALYSIS OF FLUTTER-BASED THIN-FILM CANTILEVER MICROGENERATOR

Abdul Hakim Javid[1], Raed Kafafy[2], Erwin Sulaeman[1], Sany Ihsan[1] and Moumen Idres[1]
[1]Mechanical Engineering Departmental, International Islamic University Malaysia, Kuala Lumpur, Malaysia
[2] EAU School of Engineering, Emirates Aviation University, Dubai, United Arab Emirates
E-Mail: ahjaveedindia@gmail.com

ABSTRACT

This paper presents a model for design and analysis of flutter-based microgenerators and a new concept for wind energy harvesting using thin-film cantilever with coils embedded on the sides of the cantilever. The analytical model predicts the flow-induced response of the thin-film cantilever at various parameters as well as the frequency of flutter at a wind speed which is crucial for designing a flutter based microgenerator. A complete analytical model unites various physics involved, flow induced forces on the cantilever, mechanical vibrations, electromagnetic coupling, and electric power output. The flutter frequency predicted by the analytical model is verified against finite element analysis using NASTRAN. The effect of span, width of the cantilever, length of coil on the cantilever and load resistance is investigated on the performance of the harvester. The results predicted by the analytical model agree reasonably well with the finite element analysis results paving way of using such an analytical model to design and optimize a fluttering wind energy harvester.

Keywords: energy harvesting, wind energy, flutter, microgenerator, electromagnetic induction.

INTRODUCTION

Remote monitoring applications involve sensors to monitor physical or environmental conditions, such as temperature, sound, vibration, pressure, motion or pollutants and pass their data wirelessly to a main location. Monitoring includes air pollution monitoring, forest fire detection, landslide detection, machine health monitoring and structures such as bridges, flyovers, embankments, tunnels, dams etc. Powering remote sensors is a challenge; they were initially powered by batteries. These batteries powered sensors only for a certain period. This caused the sensors to go offline running out of power after the battery life. Replacing the batteries of every sensor after its life time is not an option, since an application involves several hundred sensors in complex structures and along with that these sensors are placed in remote locations which are often very difficult to reach periodically. For example, at an average power consumption of 100 microwatts (an order of magnitude smaller than any currently available node), standard sensor node batteries must be replaced at least every nine months [1].

Wind energy which is a renewable energy source comes clean and has a power density proportional to cube of the wind speed; it promises a very good deal of energy when rightly converted. Wind energy harvesting shows a good sign in autonomous supply of power to the sensor nodes at raised locations for example bridges, dams, mountains etc. and remote locations such as wildlife sanctuaries. Since these nodes need only a small amount of power, micro generators are suitable for this purpose. Conventional method of harvesting wind with the help of wind turbine is suitable only for larger applications. For smaller applications, when wind turbines were made in small sizes it resulted in lesser efficiency because with the down scaling the moving parts had more friction compared to the rotational motion generated by the micro wind turbine.

An experimental investigation on effect of miniaturization on the efficiency of miniature windmills in the range of 1-100mW was reported. Efficiency of 1.5% was achieved with 5.5 m/s wind speed and 9.5% efficiency at 11.8 m/s using a 4.2 cm dia turbine [2]. This work explains the inability of employing miniature windmills for energy harvesting from low wind speeds.

A miniature wind turbine employing a sub Watt brushless DC motor as the generator operable between 3 – 4.5 m/s wind speed was investigated. Theoretical efficiency of 14.8% was predicted [3].

A piezoelectric windmill made of 18 piezoelectric bimorph with a cut-in wind speed of 2.4 m/s was analyzed and tested. The wind flow is converted into a rotational motion on the shaft with the cup vanes, a lever connected to the shaft hits the tip of the piezoelectric bimorph and generates an electric voltage. It generated 5 mW of continuous power at 4.4 m/s [4],[5].

Windbelt based linear vibratory micro generators contribute in scavenging energy from ambient air flow, they are able to convert ambient air flow to vibrations with the windbelt and permanent magnets embedded on it move with respect to the coil generating electrical. µicroWindbelt™ generates power output of 0.2 mW at windspeed of 3.5 m/s and 2.0 mW at 5.5 m/s with an operating frequency of 70 Hz. The membrane for this device is 12cm x 0.7cm [6].

A modified method of harvesting energy from fluttering windbelt was proposed by Fei *et al.*, they designed an electromagnetic resonator which worked like a piston inside a cylinder instead of having permanent magnets embedded into the belt. The resonator is placed near the end in the belt to make use of bending stiffness [7]. The resonator has a mass (permanent magnet) moving

between 2 coils. Two coils are placed in such an order they intersect the magnetic lines of force of the permanent magnets at various speeds and 1.3 mW of power was harvested from a wind speed of 3.1 m/s.

An aerofoil harvester with transversal and rotational motions induced due to flow is proposed by Pagwiwoko. A 0.28m long aerofoil wing flutters with an amplitude of 4mm in a limit cycle oscillation by limiting the pitching motion to 0.05 radian at a wind speed of 16.5 m/s. [8]

In another aerofoil harvester, an analysis is performed to determine the effect of eccentricity between the gravity axis and the elastic axis on the energy harvested. A piezoelectric energy harvester is employed to convert the vibration energy from the aerofoil which is suspended by a non linear springs. [9]

A flexible cantilever plate is placed in an axial flow causing it to flutter once the flow speed crosses the instability threshold. This flutter is made use for harvesting the energy from the flow. The energy transfer between the fluid flow and the flexible plate is investigated. [10]

A T-shaped cantilever with piezoelectric patches on it was designed and tested. Because of T-shaped projection its flutter characteristics is improved which results in providing power of 4 mW at 4 m/s of wind speeds[11]. In another work with T-shaped cantilever researchers demonstrated electromagnetic transduction by placing magnetic on the cantilever and coils externally. Both of these T-shaped cantilever devices worked on cross flow fluttering. A CFD code using particle vortex method was used to simulate the time response of the system. A flow augmenting funnel was also proposed in order to direct and magnify the wind flow [12].

A cantilever thin film with piezoelectric patches was proposed and its flutter and power generation characteristics compared with and without circular and square cross section bluff bodies attached to the tip. Square bluff bodies show good flutter response due to the vortices formed behind it [13].

A computational and experimental analysis was performed by placing a piezoelectric cantilever beam parallel to the flow direction at the wake of a cylinder. The presence of a cylinder in the flow creates a better aerodynamic loading on the beam because of the formation of vortices [14].

A cantilever beam like multifunctional structure, which not only acts as a load bearing aircraft wing but also as a energy harvesting device is proposed in an analysis. Piezoelectric material placed over the wing substrate harvest energy from the aerodynamic loads and can also acts as damping device when coupled to suitable electric circuits [15].

In a similar analysis, a cantilever beam with embedded piezoelectric material vibrates due to the wind-induced fluttering motion. This leaf-like beam is placed in a cross flow arrangement amplifying the magnitude of vibration [16].

A FLUTTER-BASED ELECTROMAGNETIC ENERGY HARVESTER

A micro scale electromagnetic vibration energy harvester was demonstrated with cantilever beams of various natural frequencies embedded with pickup coils moving in a magnetic field [17]. A milli scale vibration energy harvester using cantilever beams with pickup coils was demonstrated and 2.5 kW of power was generated from a single cantilever [18]. In this paper we propose a novel design of flutter-based electromagnetic energy harvester, which replaces the lengthy fluttering element proposed by Frayne [6] and Fei et al [19] by a thin film cantilever fluttering element placed in a cross flow. Also, the coils are placed on the fluttering element unlike proposed by Fei *et al.* A Nd-FeB permanent magnet is placed near the coil to create a magnetic flux around the moving coil. In this design, a number of cantilever thin films embedded with pick up coils can be placed on both sides of the magnet as shown in the figure 4. The thin film's dimension can be decided upon analysis of its fluttering characteristics and available wind speed in its application. This setup can also be placed inside a wind speed augmenting funnel for better wind flow direction control and velocity.

AERODYNAMIC FLUTTER MODEL

Mathematical models for flutter have been given by researchers who faced this as an undesirable phenomenon in bridges. Since our problem is similar to bridges, these mathematical models can be taken as governing works. Scanlan and Tomoko [20] proposed a mathematical model for flutter in simplest form considering a two degree motion, a simple sketch explaining flutter is shown in Figure-1. It shows a cantilever thin film beam suspended in a cross flow with a wind speed U. The vertical displacement made by the film on each side of its equilibrium state is denoted by H, and angular displacement as α

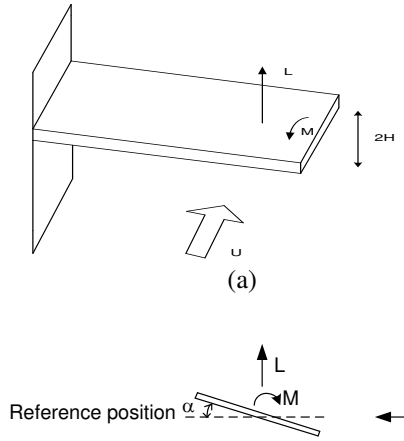

Figure-1. Illustration of the displacements and forces acting on cantilever beam. (a) sketch showing cantilever beam placed in a cross flow (b) lift and moment forces described on the cross section of the cantilever film.

A simple mathematical model for the flutter motion is given by,

$$m\ddot{h} + c_h\dot{h} + k_h h = L$$
$$I\ddot{\alpha} + c_\alpha\dot{\alpha} + k_\alpha\alpha = M \quad (1)$$

Where m is mass per unit length, I is section polar moment per unit length, c_h is vertical damping coefficient, $c_\alpha$is rotational damping coefficient, k_h and k_α vertical and rotational stiffness coefficients respectively.

In terms of critical damping ratiosζ_h, $\zeta_\alpha$and natural circular frequencies ω_h and ω_α, we can rewrite the above equations of motion as

$$\ddot{h} + 2\zeta_h\omega_h\dot{h} + \omega_h^2 h = \frac{L}{m}$$
$$\ddot{\alpha} + 2\zeta_\alpha\omega_\alpha\dot{\alpha} + \omega_\alpha^2\alpha = \frac{M}{I} \quad (2)$$

A thin airfoil or thin plane analysis in incompressible flow was proposed by Theodorsen [21], which is similar to flutter analysis of thin cantilever film carried out in our work. Theodorsen introduced aerodynamic coefficients, which are defined in terms of two theoretical functions F(k) and G(k). The complex function C(k) of which F(k) and G(k) are the real and imaginary parts, respectively, is known as Theodorsen's circulation function.

$$C(k) = F(k) + iG(k) \quad (3)$$

Where

$$F = \frac{J_1(J_1 + Y_0) + Y_1(Y_1 - J_0)}{(J_1 + Y_0)^2 + (Y_1 - J_0)^2} \quad (4)$$

$$G = -\frac{Y_1Y_0 + J_1J_0}{(J_1 + Y_0)^2 + (Y_1 - J_0)^2} \quad (5)$$

Where J_i and Y_i are Bessel functions of the first kind and second kind respectively. Scanlan [22] developed a full form of flutter derivatives for thin plane analysis which gives the lift and moment in terms of thin plane vertical and rotational displacements. The lift and moment may be expressed as

$$L = qB[KH_1^*\frac{\dot{h}}{U} + KH_2^*B\frac{\dot{\alpha}}{U} + K^2H_3^*\alpha + K^2H_4^*\frac{h}{B}]$$
$$M = qB^2[KA_1^*\frac{\dot{h}}{U} + KA_2^*B\frac{\dot{\alpha}}{U} + K^2A_3^*\alpha + K^2A_4^*\frac{h}{B}] \quad (6)$$

Where q is the dynamic pressure of wind = 1/2 ρU^2, B is the width of the film and K is the reduced frequency = ωB/U. The aeroelastic flutter derivatives are only valid for harmonic solutions which can be found at the onset of the flutter phenomenon [23]. Therefore, the oscillatory transverse and rotational displacements can be described by

$$h = h_0e^{i\omega t}$$
$$\alpha = \alpha_0e^{i(\omega t+\theta)} \quad (7)$$

Where $i = \sqrt{-1}$, ω is the solution frequency (flutter frequency), h_0 is the amplitude of the transverse oscillations, α_0 is the amplitude of the rotational oscillations, and θ is the phase shift between the transverse and rotational oscillations.

DETERMINING THE FLUTTER FREQUENCY

The flutter frequency referred to in this paper is the frequency of vibration of the fluttering cantilever at the tip, which should not be confused with flutter speed, which is the wind speed at which the fluttering onsets. This onset of flutter wind speed is important in designing a harvester for the available source of wind, and the flutter frequency translates the power harvest of the fluttering cantilever. The energy harvested from the fluttering cantilever is determined from the flutter frequency, since the power harvested is directly proportional to the frequency of vibration of the harvester.

We propose a simple method to solve (Equation 2) for the flutter frequency of the fluttering cantilever at any given condition of wind speed and cantilever geometry. The aeroelastic lift and moment acting on the fluttering cantilever are given by Scanlan's model in terms of the transverse and rotational displacements and their derivatives (Equation 6). Substituting the aeroelastic lift and moment from (Equation 6) into (Equation 2), we get.

$$\ddot{h} + 2\zeta_h\omega_h\dot{h} + \omega_h^2 h = \frac{qB}{m}[KH_1^*\frac{\dot{h}}{U} + BKH_2^*\frac{\dot{\alpha}}{U} + K^2H_3^*\alpha + \frac{K^2}{B}H_4^*h] \quad (8)$$

$$\ddot{\alpha} + 2\zeta_\alpha\omega_\alpha\dot{\alpha} + \omega_\alpha^2\alpha = \frac{qB^2}{I}[KA_1^*\frac{\dot{h}}{U} + BKA_2^*\frac{\dot{\alpha}}{U} + K^2A_3^*\alpha + \frac{K^2}{B}A_4^*h] \quad (9)$$

Since the aeroelastic flutter derivatives are only valid for harmonic solutions which can be found at the onset of the flutter phenomenon, so we assume the oscillatory transverse and rotational displacements of the fluttering cantilever are given by (Equation 7). Substituting (Equations 7) into (Equation 8 and (Equation 9), then dividing the resulting equations by e^iωt, we get

$$-h_0\omega^2 + 2\zeta_h\omega_h h_0 i\omega + \omega_h^2 h_0 = \frac{qB}{m}\left[KH_1^*\frac{i\omega h_0}{U} + BKH_2^*\frac{i\omega e^{i\theta}\alpha_0}{U} + K^2H_3^* e^{i\theta}\alpha_0 + \frac{K^2}{B}H_4^* h_0\right] \quad (10)$$

$$-\alpha_0\omega^2 e^{i\theta} + 2\zeta_\alpha\omega_\alpha\alpha_0 i\omega e^{i\theta} + \omega_\alpha^2\alpha_0 e^{i\theta} = \frac{qB^2}{I}\left[KA_1^*\frac{i\omega h_0}{U} + BKA_2^*\frac{i\omega e^{i\theta}\alpha_0}{U} + K^2A_3^* e^{i\theta}\alpha_0 + \frac{K^2}{B}A_4^* h_0\right] \quad (11)$$

Separating the real and imaginary parts in the above equations, we get

Re (Equation 10):

$$-h_0\omega^2 + \omega_h^2 h_0 = -qB^2KH_2^*\frac{\alpha_0\omega\sin\theta}{mU} + qBK^2H_3^*\frac{\alpha_0\cos\theta}{m} + qK^2H_4^*\frac{h_0}{m} \quad (12)$$

Im(Equation 10):

$$2\zeta_h\omega_h h_0\omega = qBKH_1^*\frac{h_0\omega}{mU} + qB^2KH_2^*\frac{\alpha_0\omega\cos\theta}{mU} + qBK^2H_3^*\frac{\alpha_0\sin\theta}{m} \quad (13)$$

Re(Equation 11):

$$-\omega^2\alpha_0\cos\theta - 2\zeta_\alpha\omega_\alpha\alpha_0\omega\sin\theta + \omega_\alpha^2\alpha_0\cos\theta = -qB^3KA_2^*\frac{\alpha_0\omega\sin\theta}{IU} + qB^2K^2A_3^*\frac{\alpha_0\cos\theta}{I} + qBK^2A_4^*\frac{h_0}{I} \quad (14)$$

Im(Equation 11):

$$-\omega^2\alpha_0\sin\theta + 2\zeta_\alpha\omega_\alpha\alpha_0\omega\cos\theta + \omega_\alpha^2\alpha_0\sin\theta = qB^2KA_1^*\frac{h_0\omega}{IU} + qB^3KA_2^*\frac{\alpha_0\omega\cos\theta}{IU} + qB^2K^2A_3^*\frac{\alpha_0\sin\theta}{I} \quad (15)$$

Dividing equations (12)–(15) by ω^2 and substituting $\frac{K}{\omega} = \frac{B}{U}$, then simplifying we get .

$$C_{11}h_0 = (C_{12}\sin\theta + C_{13}\cos\theta)\alpha_0 \quad (16)$$

$$C_{21}h_0 = (C_{22}\sin\theta + C_{23}\cos\theta)\alpha_0 \quad (17)$$

$$C_{31}h_0 = (C_{32}\sin\theta + C_{33}\cos\theta)\alpha_0 \quad (18)$$

$$C_{41}h_0 = (C_{42}\sin\theta + C_{43}\cos\theta)\alpha_0 \quad (19)$$

Dividing (Equation 16) by (Equation 17) and (Equation 18) by (Equation 19), we get.

Where

$$C_{11} = -1 + \left(\frac{\omega_h}{\omega}\right)^2 - \frac{q}{m}\frac{B^2}{U^2}H_4^*,$$
$$C_{12} = -\frac{q}{m}\frac{B^3}{U^2}H_2^*,\ C_{13} = \frac{q}{m}\frac{B^3}{U^2}H_3^*$$
$$C_{21} = 2\zeta_h\left(\frac{\omega_h}{\omega}\right) - \frac{q}{m}\frac{B^2}{U^2}H_1^*,$$
$$C_{22} = \frac{q}{m}\frac{B^3}{U^2}H_3^*,\ C_{23} = \frac{q}{m}\frac{B^3}{U^2}H_2^*$$
$$C_{31} = \frac{q}{I}\frac{B^3}{U^2}A_4^*,\ C_{32} = -2\zeta_\alpha\frac{\omega_\alpha}{\omega} + \frac{q}{I}\frac{B^4}{U^2}A_2^*,$$
$$C_{33} = -1 + \left(\frac{\omega_\alpha}{\omega}\right)^2 - \frac{q}{I}\frac{B^4}{U^2}A_3^*$$
$$C_{41} = \frac{q}{I}\frac{B^3}{U^2}A_1^*, C_{42} = -1 + \left(\frac{\omega_\alpha}{\omega}\right)^2 - \frac{q}{I}\frac{B^4}{U^2}A_3^*,$$
$$C_{43} = 2\zeta_\alpha\left(\frac{\omega_\alpha}{\omega}\right) - \frac{q}{I}\frac{B^4}{U^2}A_2^*$$

$$\frac{C_{11}}{C_{21}} = \frac{C_{12}\sin\theta + C_{13}\cos\theta}{C_{22}\sin\theta + C_{23}\cos\theta} = \frac{C_{12}\tan\theta + C_{13}}{C_{22}\tan\theta + C_{23}} \quad (20)$$

$$\frac{C_{31}}{C_{41}} = \frac{C_{32}\sin\theta + C_{33}\cos\theta}{C_{42}\sin\theta + C_{43}\cos\theta} = \frac{C_{32}\tan\theta + C_{33}}{C_{42}\tan\theta + C_{43}} \quad (21)$$

Now, solving (Equation 20) for $\tan\theta = \phi_1$, we get and solving (Equation 21) for $\tan\theta = \phi_2$, we get.

$$\phi_2 = \tan\theta = \frac{C_{41}C_{33} - C_{31}C_{43}}{C_{31}C_{42} - C_{41}C_{32}} = \frac{A_1^*\left[1 - \left(\frac{\omega_\alpha}{\omega}\right)^2 + \frac{q}{I}\frac{B^4}{U^2}A_3^*\right] + A_4^*\left[2\zeta_\alpha\left(\frac{\omega_\alpha}{\omega}\right) - \frac{q}{I}\frac{B^4}{U^2}A_2^*\right]}{A_4^*\left[1 + \left(\frac{\omega_\alpha}{\omega}\right)^2 + \frac{q}{I}\frac{B^4}{U^2}A_3^*\right] - A_1^*\left[2\zeta_\alpha\left(\frac{\omega_\alpha}{\omega}\right) + \frac{q}{I}\frac{B^4}{U^2}A_2^*\right]} \quad (22)$$

The solution frequency or the fluttering frequency is the frequency that will result in $\phi_1 = \phi_2$ at flutter. Graphically, this is the frequency (or frequencies) at which the functions ϕ_1 and ϕ_2 intersect. Numerically, the solution frequency (or frequencies) can be found by solving the equation $[\phi_1 - \phi_2 = 0]$. Using this simple technique one can easily find out the frequency of the thin film at any given wind speed and fluttering cantilever geometry. This can also be used to predict the flow induced response of a windbelt or other similar thin plane objects placed in the wind which is necessary in the parametric design of fluttering wind energy harvesters.

To demonstrate the above formulation, the functions ϕ_1 and ϕ_2 are plotted over a wide range of frequencies (0 – 4500 rad/s). The plot in Figure-2 shows

response of these two dimensionless variables to iterations with respect to angular frequency of flutter. These two curves intersect each another first at a frequency of 15.33 rad/sec which can be understood as the response frequency of the structure to the wind speed and when iterated over a wide range of frequency if is found that they intersect each other again few more times. With the proposed analytical model, it is predicted that this cantilever film will flutter with an angular frequency of 15.33 rad/sec when placed in a 2 m/s cross flow wind.

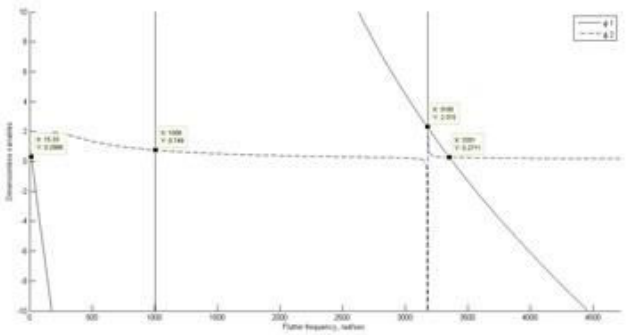

Figure-2. Graphical representation of the technique used to solve for the fluttering frequency.

A PET cantilever film 2cm wide, 6cm long and 0.1mm thick is analyzed with our flutter frequency determination model across various incident wind speeds and the 3 points of intersections of the dimensionless variables are tabled below.

Table-1. First three fluttering frequencies as predicted by the fluttering model at varied wind speeds.

Wind speed (m/s)	ω_1 (rad/s)	ω_2 (rad/s)	ω_3 (rad/s)
2	15.39	401.39	833.84
4	30.94	403.91	774.01
6	46.79	407.96	723.24
8	63.12	413.41	692.95

The first point of intersection of the two dimensionless variables gives us the flutter frequency of the cantilever film for the particular wind speed. Also, this is explained by the increase in trend of the 1st point values from 15.39 rad/s to 63.12 rad/s when the wind speed is increased from 2 to 8 m/s.

ELECTROMAGNETIC GENERATOR MODEL

In this work, we propose flutter-based microgenerator with coils embedded on the surface of a vibrating belt (or film) which can be optimized to work over a wide range of frequencies. A thin electric coil shall be etched over the belt surface in a loop with electric load connected to it. Coils can be embedded on both sides of the belt depending on the optimized mass influence of the coils to the vibrating belt. The mass of the coil can be found from the lift force induced in the vibrating belt.

As shown in the Figure-3.a thin films of varying length are attached to a structure. These lengths can be finalized with their characteristic vibration reaction to air flow, to accommodate a wide range of environmental wind speeds. Each of the suspended films may have its own resonance frequency at a particular wind speed, and rest of the suspended films will vibrate with respect to their resonance frequencies. These suspended films shall be embedded with coil turns on both the sides, which move with respect to a magnetic field B. The basic mathematical model can be applied for different sets of coils.

$$R_c = \frac{N.L_{MT}}{\sigma_{coil} A_{wire}} \tag{23}$$

Where $\sigma_{coil}$the conductance of the coil wire, N is is the number of turns and LMT is length of mean turn.

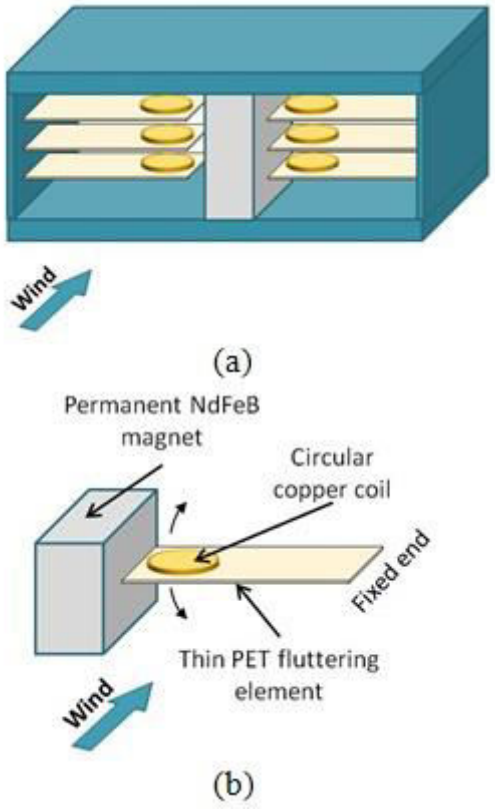

Figure-3. Proposed setup of cantilever film with pick up coils embedded on to the surface (a) arrangement of three different sets of cantilever stacked around a magnet; (b) cantilever film placed near a magnet.

The coil inductance is assumed to be much smaller than the internal resistance of the coil. The power delivered to the resistive load RL can be obtained from

$$P = \frac{1}{2} i^2 R_L \tag{24}$$

The induced current iis given by

$$i = \frac{V}{R_L + R_C} \tag{25}$$

$$V = -\frac{d\Phi}{dt} = -\frac{d}{dt}\left(\int B.\,dA\right) = -BL_C\dot{h} \tag{26}$$

The magnetic field strength spatial distribution is given by [24]

$$B = \frac{B_r}{\pi}\left[\tan^{-1}\left(\frac{a_1 a_2}{2d\sqrt{a_1^2 + a_2^2 + 4d^2}}\right) - \tan^{-1}\left(\frac{a_1 a_2}{2(d + a_p)\sqrt{a_1^2 + a_2^2 + 4(d + a_p)^2}}\right)\right] \tag{27}$$

Br is the residual magnetic flux density (1 – 1.5T for NdFeB type magnets), ap is the length of the magnet through magnetized direction, a1 is the height of magnet, a2 is the width of the magnet, and d is the distance from the magnet. The relative velocity $\dot{h}$ can be calculated from the flutter model.

$$P = \frac{R_L}{2(R_L + R_C)} iV \tag{28}$$

We can find P_{rms} from

$$P_{rms} = \frac{R_L}{2(R_L + R_C)} i_{rms} V_{rms} = \frac{R_L}{2(R_L + R_C)^2}(V_{rms})^2 = \frac{R_L L_C^2 B^2}{4(R_L + R_C)^2} h_0^2 \omega^2 \tag{29}$$

From which it is obvious that power output is proportional to the square of flutter frequency. The damping experienced by the vibrating film can be divided into two components, mechanical damping and the electrical damping [17]. Mechanical damping is generated from the air flow and mechanical properties of the material.

$$b_m = b_{air} + b_{material} \tag{30}$$

The components of air flow damping c_h, c_α, ζ_h and $\zeta_\alpha$are considered in the flutter model earlier in equation. (1) and (2), so they will not be considered here. Then, the mechanical damping is simply material damping which can be expressed as[25]

$$b_m = b_{material} = \frac{\eta}{\omega} k_{eq} + \frac{(0.23h^3)}{S^3} 2m_{eq}\omega_h \tag{31}$$

where η is the structural damping coefficient determined by the material properties, ω is the displacement frequency of the tip point of the cantilever, ω_h is the natural frequency of the cantilever in transverse motion, m_{eq} is the equivalent mass and k_{eq} is the equivalent stiffness of the cantilever. The values of m_{eq} and k_{eq} are given by [26]

$$m_{eq} = \frac{33}{140} m \tag{32}$$

$$k_{eq} = \frac{3EI}{S^3} \tag{33}$$

The electrical damping b_e is given by

$$b_e = \frac{(d\Phi/dh)^2}{R_L + R_C} = \frac{(BL_e)^2}{R_L + R_C} \tag{34}$$

The optimal load resistance to maximize load power, can be calculated from [27].

$$\zeta_{eq} = \zeta_m + \zeta_e = \frac{b_m + b_e}{2m_{eq}\omega_h} = \frac{b_{eq}}{2m_{eq}\omega_h} \tag{35}$$

Table-2. Parameters used for simulation.

Parameter	Values
NdFeB magnet, L x W x H	2 x 2 x 5 cm
Br, residual magnetism	1.3 T, Grade N49
Length of copper wire	50 m
Insulated copper wire gauge	45 G
Resistance per metre of 45G wire	10.98 Ohm
Distance between the magnet wall and centre of coil	1.1 cm
Load resistance	500 Ohm

SIMULATION

A MATLAB code based on the flutter frequency determination model discussed above was developed to determine the value of flutter frequency at various wind speeds, geometries and electromagnetic induction considering mechanical and electric damping. A variety of cantilever dimensions are considered and their flutter frequency and electrical output are examined at various wind speeds. An investigation on change in span, width, coil turns and load resistance change is also performed. A bar magnet is considered for simulation, whose magnetic field strength can be calculated from equation (21). The coil is assumed to have constant flux cut at all the positions during flutter.

The analytical model was tested for various cantilever geometries, number of coil turns, load resistance and different wind speeds. For width b = 4cm, thickness =

0.1mm of the cantilever film, load resistance of 10Ohm, magnetic field of 0.1835T, with 30m of copper coil wound on both the sides. The span of the film is varied from 3cm to 7cm to study the response at wind speeds of 10 and 15m/s.

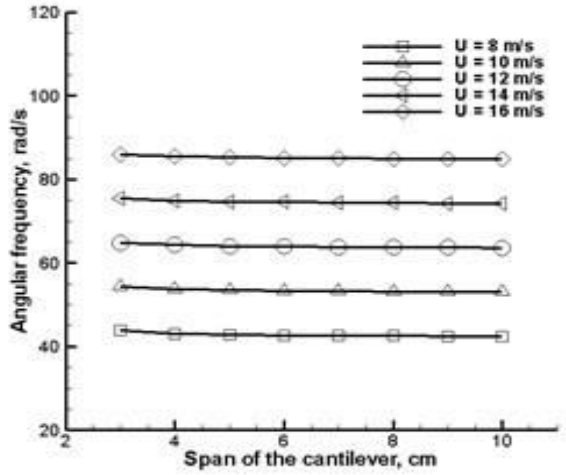

Figure-4. Effect of change in span of the cantilever on the response frequency at two wind speeds.

Similarly, the width is varied from 2cm to 5cm by fixing length at 6cm and all the other parameters as discussed above.

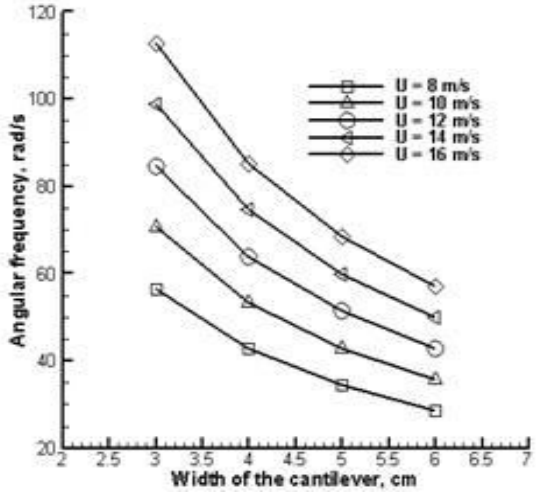

Figure-5. Effect of change in width of the cantilever on the response frequency at two wind speeds.

The length of copper wire used in winding is varied from 10 to 50m to study the effect of coil mass and electrical damping offered to the flow induced response. 45G insulated copper wire is considered for simulation. Other parameters are fixed as discussed above.

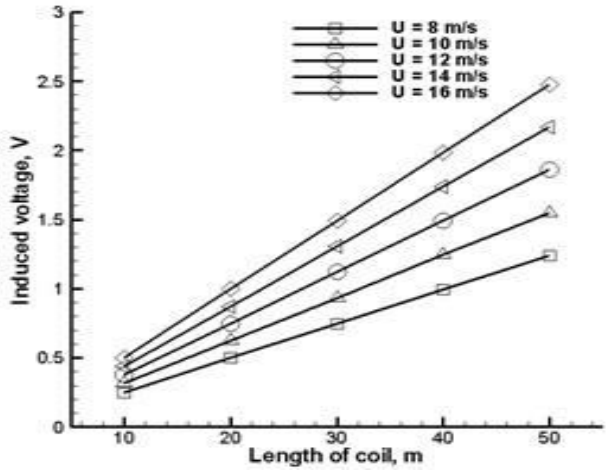

Figure-6. Effect of change in length of coil winding on the cantiever surface against frequency response at two wind speed.

The load resistance is varied from 10 to 105 Ohm to determine the effect of electrical loading on the flutter microgenerator. For the coil and film parameters as discussed above, the current drops due to the increase in load resistance and the power generated by the harvester is plotted against the load resistance connected.

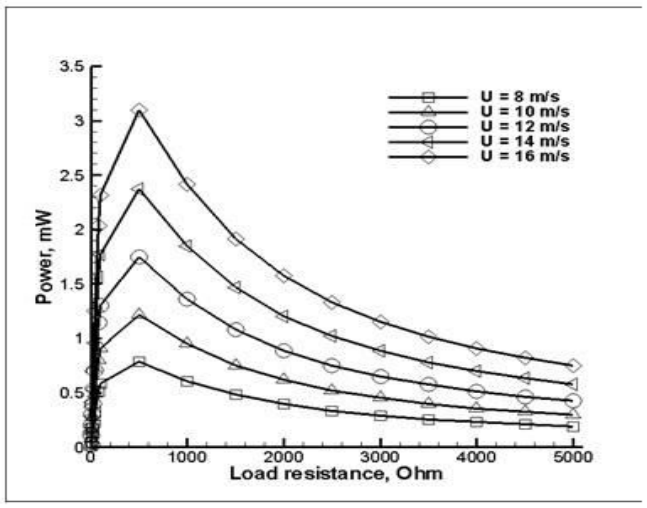

Figure-7. Effect of change in load resistance connected to the coils on the cantilever on the current.

Similarly, a Nastran FEA simulation was attempted to investigate the closeness to the analytical prediction of the flow induced response on the thin film. A simple case was tried, a 2cm x 5cm polyethylene teraphthalate (PET) plate of 0.1mm thickness, Youngs' Modulus 2GPa, density of PET 1300kg/m3. PK flutter method was selected for solving flow induced response of the plate. The structure mesh was made as such the cantilever element is divided into 8 and 20 units in the X and Y axes respectively of 2.5mm each side. The beam is configured to have fixed-free-free-free ends. Flutter can occur in any or in combinations of various mode shapes.

The first five mode shapes of vibration occurring in the beam are shown in Figure-9. The eigen values of tip displacement are computed along with each mode shape's deformation. The prediction of the occurrence of flutter in carried out by investigating the damping coefficients of the first five modes.

From the simulation conducted at Nastran, the flutter condition is identified by observing the change in sign of the structural damping at varied wind speeds. A cantilever plate of width 2cm, length 5cm and thickness 0.1mm is considered for simulation. At the point of flutter, the frequencies of structural vibration at various modes are identified. The plot below shows structural damping curves for the first 5 modes of vibration occurring at the plate with change in wind speed. Out of the 5 curves, mode shape number 4 shows a characteristic behavior. It clearly crosses the zero mark after offering negative damping to the structure for quite a while, with this change in sign of the damping force it is predicted that the onset of flutter occurs at 10m/sec wind speed.

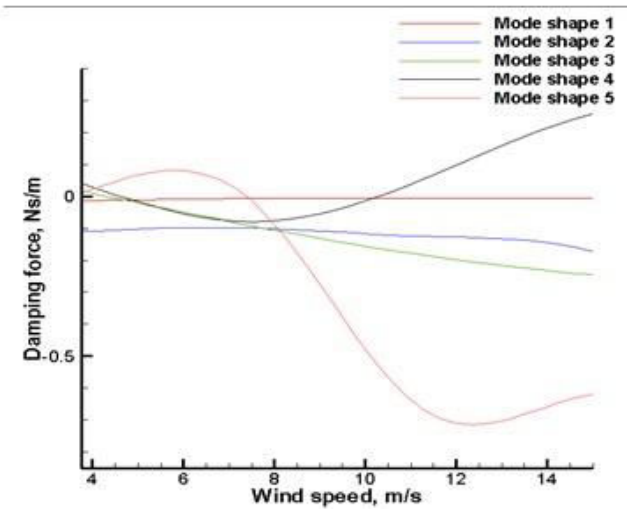

Figure-8. Damping force offered by the structure at various wind speeds for the first five mode shapes of vibration.

The structural vibration frequency at various wind speeds are studied from Nastran results, it is shown in the plot below. From the structural damping results we know the structure reaches the flutter condition at 10m/sec and continues to flutter hereafter with increased amplitudes. The mode shapes 4 and 5 seem to flutter with little difference in frequency.

Comparing the Nastran simulation results with the proposed analytical model at 10m/sec for the same geometry, the analytical model gives us an output of 168Hz flutter frequency and Nastran simulation results gives a frequency148Hz. These two frequencies are closer to each another at the point of flutter.

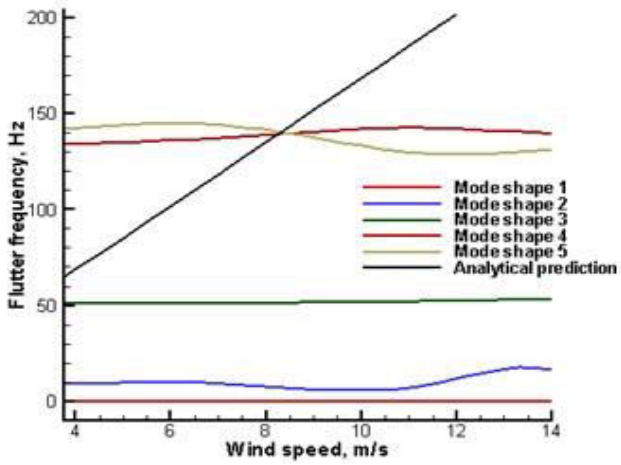

Figure-9. Frequencies of flutter at various wind speeds for the first five mode shapes of vibration.

CONCLUSIONS

In this paper, the performance of a flutter-based thin-film cantilever microgenerator with coils on the cantilever is assessed using analytical modeling and finite element analysis. The analytical model developed incorporates the aeroelastic interaction between the thin-film cantilever and the wind as well as the electromagnetic induction in the vibrating coils. An analytical method to determine the fluttering frequency of the cantilever at given wind speed and cantilever configurations – is introduced. Analytical solutions show that the increase in span of the cantilever from 3cm to 10cm does not have significant effect on the frequency of flutter whereas the increase in the cantilever width from 3cm to 6cm drastically reduces the frequency of flutter from 56rad/s to 28rad/s. This reduction in flutter frequency is because of higher structural damping resisting the induced aerodynamic forces. It was also found that increasing the length of the pickup coil embedded on the cantilever film from 10m to 50m increases the induced voltage proportionally. However, it increases the mass near the tip of the cantilever. It was also found that the power generated by the harvested increases with the load resistance and reaches a near saturation point at higher loads. The generated power as a peak output power of 3.1mW at 16m/s wind speed. The FEA analysis performed using NASTRAN demonstrates the cantilever beam flutters with a frequency of 148Hz at 10m/s wind speed, whereas the analytical model predicts the flutter frequency to be 168Hz, which is close enough to the FEA value.

ACKNOWLEDGEMENTS

This research work is supported by the Ministry of Higher Education, Malaysia through research grant FRGS 11-044-0193.

REFERENCES

[1] Roundy S., Wright P. K. and Rabaey J. M. 2003, "A study of low level vibrations as a power source for

wireless sensor nodes," Comput. Commun., 26(11), pp. 1131–1144.

[2] Rancourt D., Tabesh A., and Fréchette L. G., 2007, "Evaluation of centimeter-scale micro windmills: aerodynamics and electromagnetic power generation," Proc. PowerMEMS, pp. 93–96.

[3] Xu F. J., Yuan F. G., Hu J. Z., and Qiu Y. P., 2010, "Design of a miniature wind turbine for powering wireless sensors," Proceedings of SPIE, M. Tomizuka, ed., p. 764741.

[4] Myers R., Vickers M., Kim H., and Priya S., 2007, "Small scale windmill," Appl. Phys. Lett., 90(5), p. 054106.

[5] Priya S., 2005, "Modeling of electric energy harvesting using piezoelectric windmill," Appl. Phys. Lett., 87(18), p. 184101.

[6] 2011, "Humdinger Wind Energy" [Online]. Available: http://www.humdingerwind.com.

[7] Fei F., and Li W. J., 2009, "A fluttering-to-electrical energy transduction system for consumer electronics applications," 2009 IEEE International Conference on Robotics and Biomimetics ROBIO, pp. 580–585.

[8] Pagwiwoko C. P., 2013, "Limit Cycle Oscillation Analysis on the Design of Wind Power Harvester with Fluttering Aerofoil," International Conference on Renewable Energies and Power Quality (ICREPQ'13).

[9] Abdelkefi a., Nayfeh a. H., and Hajj M. R., 2011, "Enhancement of power harvesting from piezoaeroelastic systems," Nonlinear Dyn., 68(4), pp. 531–541.

[10] Tang L., Païdoussis M. P., and Jiang J., 2009, "Cantilevered flexible plates in axial flow: Energy transfer and the concept of flutter-mill," J. Sound Vib., 326(1-2), pp. 263–276.

[11] Kwon S.-D., 2010, "A T-shaped piezoelectric cantilever for fluid energy harvesting," Appl. Phys. Lett., 97(16), p. 164102.

[12] Park J., Morgenthal G., Kwon S., and Law K., 2012, "Power evaluation for flutter-based electromagnetic energy harvester using CFD simulations," First International Conference on Performance-based and Life-cyle Structural Engineering (PLSE 2012).

[13] Gao X., 2011, "Vibration and Flow Energy Harvesting using Piezoelectric," Drexel University.

[14] Akaydin H. D., Elvin N., and Andreopoulos Y., 2010, "Energy Harvesting from Highly Unsteady Fluid Flows using Piezoelectric Materials," J. Intell. Mater. Syst. Struct., 21(13), pp. 1263–1278.

[15] De Marqui C., Vieira W. G. R., Erturk A., and Inman D. J., 2011, "Modeling and Analysis of Piezoelectric Energy Harvesting From Aeroelastic Vibrations Using the Doublet-Lattice Method," J. Vib. Acoust., 133(1), p. 011003.

[16] Li S., Yuan J., and Lipson H., 2011, "Ambient wind energy harvesting using cross-flow fluttering," J. Appl. Phys., 109(2), p. 026104.

[17] Sari I., Balkan T., and Kulah H., 2008, "An electromagnetic micro power generator for wideband environmental vibrations," Sensors Actuators A Phys., 145-146, pp. 405–413.

[18] Kulah H., and Najafi K., 2004, "An electromagnetic micro power generator for low-frequency environmental vibrations," Micro Electro Mech. Syst., pp. 237–240.

[19] Fei F., Mai J. D., and Li W. J., 2012, "A wind-flutter energy converter for powering wireless sensors," Sensors Actuators A Phys., 173(1), pp. 163–171.

[20] Scanlan R. H., and Tomko J. J., 1971, "Airfoil And Bridge Deck Flutter Derivatives," J. Eng. Mech. Div., 97(6), pp. 1717–1737.

[21] Theodorsen T., 1949, General theory of aerodynamic instability and the mechanism of flutter, NACA Technical report no.496.

[22] Simiu E., and Scanlan R. H., 1996, Wind effects on structures - Fundamentals and applications to design, Wiley.

[23] Starossek U., and Aslan H., 2009, "Experimental and numerical identification of flutter derivatives for nine bridge deck sections," Wind Struct., 12(6), pp. 519–540.

[24] Mizuno M., and Chetwynd D. G., 2003, "Investigation of a resonance microgenerator," J. Micromechanics Microengineering, 13(2), pp. 209–216.

[25] Hosaka H., Itao K., and Kuroda S., "Evaluation of energy dissipation mechanisms in vibrational microactuators," Proceedings IEEE Micro Electro Mechanical Systems An Investigation of Micro Structures, Sensors, Actuators, Machines and Robotic Systems, IEEE, pp. 193–198.

[26] Rao S. S., 2005, Mechanical Vibrations, Pearson-Prentice Hall.

[27] Beeby S. P., and O'Donnell T., 2009, "Electromagnetic Energy Harvesting," Energy Harvesting Technologies, S. Priya, and D.J. Inman, eds., Springer US.